Evaluating soil moisture retrievals from ESA's SMOS and NASA's SMAP brightness temperature datasets

A. Al-Yaari[1], **J.-P. Wigneron**[1], **Y. Kerr**[2], **N. Rodriguez-Fernandez**[2], **P. E. O'Neill**[3], **T. J. Jackson**[4], **G.J.M. De Lannoy**[5], **A Al Bitar**[2], **A. Mialon**[2], **P. Richaume**[2], **JP Walker**[6], **A. Mahmoodi**[2], and **S. Yueh**[7]

[1]INRA, UMR1391 ISPA, Villenave d'Ornon, France

[2]CESBIO, CNES/CNRS/IRD/UPS, UMR 5126, Toulouse, France

[3]NASA, Goddard Space Flight Center, Greenbelt, MD 20771, USA

[4]USDA-ARS Hydrology and Remote Sensing Laboratory, Beltsville, MD 20705-2350 USA

[5]KU Leuven, Department of Earth and Environmental Sciences, Heverlee, Belgium

[6]Department of Civil Engineering, Monash University, Clayton, Melbourne, Victoria, Australia

[7]Jet Propulsion Lab., California Inst. of Technol., Pasadena, CA, USA

Abstract

Two satellites are currently monitoring surface soil moisture (SM) using L-band observations: SMOS (Soil Moisture and Ocean Salinity), a joint ESA (European Space Agency), CNES (Centre national d'études spatiales), and CDTI (the Spanish government agency with responsibility for space) satellite launched on November 2, 2009 and SMAP (Soil Moisture Active Passive), a National Aeronautics and Space Administration (NASA) satellite successfully launched in January 2015. In this study, we used a multilinear regression approach to retrieve SM from SMAP data to create a global dataset of SM, which is consistent with SM data retrieved from SMOS. This was achieved by calibrating coefficients of the regression model using the CATDS (Centre Aval de Traitement des Données) SMOS Level 3 SM and the horizontally and vertically polarized brightness temperatures (TB) at 40° incidence angle, over the 2013 – 2014 period. Next, this model was applied to SMAP L3 TB data from Apr 2015 to Jul 2016. The retrieved SM from SMAP (referred to here as SMAP_Reg) was compared to: (i) the operational SMAP L3 SM (SMAP_SCA), retrieved using the baseline Single Channel retrieval Algorithm (SCA); and (ii) the operational SMOSL3 SM, derived from the multiangular inversion of the L-MEB model (L-MEB algorithm) (SMOSL3). This inter-comparison was made against *in situ* soil moisture measurements from more than 400 sites spread over the globe, which are used here as a reference soil moisture dataset. The *in situ* observations were obtained from the International Soil Moisture Network (ISMN; https://ismn.geo.tuwien.ac.at/) in North of America (PBO_H2O, SCAN, SNOTEL, iRON, and USCRN), in Australia (Oznet), Africa (DAHRA), and in Europe (REMEDHUS, SMOSMANIA, FMI, and RSMN). The agreement was analyzed in terms of four classical statistical criteria: Root Mean Squared Error (RMSE), Bias, Unbiased RMSE

amen.alyaari@bordeaux.inra.fr, tel: 33 5 57 12 24 27, Fax: 33 5 57 12 24 20.

(UnbRMSE), and correlation coefficient (R). Results of the comparison of these various products with *in situ* observations show that the performance of both SMAP products i.e. SMAP_SCA and SMAP_Reg is similar and marginally better to that of the SMOSL3 product particularly over the PBO_H2O, SCAN, and USCRN sites. However, SMOSL3 SM was closer to the *in situ* observations over the DAHRA and Oznet sites. We found that the correlation between all three datasets and *in situ* measurements is best (R > 0.80) over the Oznet sites and worst (R = 0.58) over the SNOTEL sites for SMAP_SCA and over the DAHRA and SMOSMANIA sites (R= 0.51 and R= 0.45 for SMAP_Reg and SMOSL3, respectively). The Bias values showed that all products are generally dry, except over RSMN, DAHRA, and Oznet (and FMI for SMAP_SCA). Finally, our analysis provided interesting insights that can be useful to improve the consistency between SMAP and SMOS datasets.

Keywords

SMOS; SMAP; soil moisture; statistical regression

1. Introduction

Lately, the importance of soil moisture has become increasingly apparent, because soil moisture is a key variable in better understanding of the land-atmosphere interactions (Chen et al., 2016; Hirschi et al., 2014). The exchange of heat and water between the land surface and atmosphere is influenced by soil moisture (Berg et al., 2014; Hupet & Vanclooster, 2002; Seneviratne et al., 2010; Western et al., 2004), which was recognized as an Essential Climate Variables (ECV) in 2010 (GCOS, 2010).

Global soil moisture information has become available via different active and passive microwave remote sensing techniques with good temporal and spatial resolutions (Bartalis et al., 2007; Kerr et al., 2001; Njoku et al., 2002; Njoku et al., 2003; Owe et al., 2001; Ulaby et al., 1996; Wigneron et al., 1995). However, the required temporal and spatial resolutions strongly depend on the applications (e.g., agricultural applications vs. climate studies). Recently, new global soil moisture datasets, with a typical target accuracy of 0.04 m^3/m^3 (Jackson et al., 2016; Kerr et al., 2010; Kerr et al., 2012) over bare, low vegetation cover, and sparsely vegetated areas, have been produced based on microwave satellite observations at L-band (1.4 GHz, 21 cm). L-band is considered optimal for soil moisture monitoring (Kerr et al., 2001; Njoku et al., 2003; Wang & Choudhury, 1981) due to its higher sensitivity to soil moisture and penetration into vegetation and soil (Kerr, 2007; Njoku et al., 2003; Owe & Van de Griend, 1998; Wang & Choudhury, 1981) than other higher frequencies (e.g., C-band, X-band, etc.). The new L-band based datasets include surface soil moisture from two spaceborne missions: ESA's (European Space Agency) Soil Moisture and Ocean Salinity (SMOS) (Kerr et al., 2012) and NASA's (National Aeronautics and Space Administration) Soil Moisture Active Passive (SMAP) (Entekhabi et al., 2010). The SMOS and SMAP satellites were launched in 2009 and 2015, respectively, and have been providing microwave brightness temperature (TB) observations since then. Soil moisture information is retrieved from SMAP's and SMOS's TB observations based on the principle that soil TB is mainly determined by soil moisture via soil dielectric constant (Njoku et al., 2002;

Schmugge et al., 1976; Ulaby et al., 1996). Nevertheless, the sensitivity of the SMOS and SMAP TB observations to soil moisture is reduced by perturbing factors such as vegetation (attenuation of the emission from the soil and additional upwelling emission toward the space-borne sensor), surface roughness (scattering effects increase the emitting surface area), topography, soil texture, soil bulk density, and soil temperature (Choudhury et al., 1979; Grant et al., 2008; Holmes et al., 2006; Jackson & Schmugge, 1991; Kerr et al., 2012; Njoku & Li, 1999; Njoku et al., 2003; Wang et al., 1983; Wigneron et al., 2007; Wigneron et al., 2011).

There are several remotely sensed soil moisture products available (in addition to SMOS and SMAP); however, these cover different periods and are not consistent in terms of spatial and temporal resolutions, period availability, grid, etc. Given the wide availability of soil moisture datasets retrieved from different microwave observations, studies focusing on the merging of these products are important to advance in the field of producing long-term and consistent datasets of several climatic variables. A great effort has been made by the scientific community in the last decade to build a coherent and consistent long term soil moisture datasets such as the ESA Climate Change Initiative (CCI) soil moisture data record (e.g., Enenkel et al., 2015; Liu et al., 2012; http://www.esa-soilmoisture-cci.org/; Wagner et al., 2012), deemed necessary for global soil moisture monitoring, drought monitoring, climate forecasts, etc. The CCI product is estimated based on a posteriori merging i.e. merging the retrieved soil moisture datasets based on the relative errors of soil moisture products and a CDF (cumulative distribution function)-matching used to rescale the different soil moisture products into a common climatology. An alternative approach is to use data fusion i.e. merging of microwave datasets prior to the retrieval (e.g., through the use of a common retrieval algorithm as proposed later in this paper). This method allows better exploitation of the complimentary of information provided by the different sensors not included in the posteriori combination approach (Aires et al., 2012; Kolassa et al., 2013). A recent project was established by ESA to investigate the integration of SMOS soil moisture estimates within the CCI soil moisture data record using three approaches that implement the data fusion strategy:

(i) multi-linear regression (Al-Yaari et al., 2016);

(i) neural networks (Rodríguez-Fernández et al., 2015); and

(ii) the Land Parameter Retrieval Model (LPRM; Van der Schalie et al., 2016).

Al-Yaari et al. (2016), for instance, demonstrated the efficiency of physically-based multiple-linear regression equations (Wigneron et al., 2004), referred to here as Linear Regression Method (LRM) in the following, to retrieve soil moisture from the Advanced Microwave Scanning Radiometer Earth Observing System (AMSR-E) TB observations. The LRM has several advantages: quickness, simplicity, and no strong demand on auxiliary datasets (Al-Yaari et al., 2016) such as the normalized difference vegetation index (NDVI) product used by the SMAP Single Channel Algorithm (SMAP_SCA), to estimate vegetation effects. The purpose of that initial study was to extend the SMOS soil moisture product into the past i.e., 2003–2009, using AMSR-E TB observations. The current study follows the same strategy to retrieve soil moisture from SMAP TB observations (SMAP_Reg) with a purpose to improve the temporal sampling rate together with the SMOS soil moisture

product at the global scale. The main interest in the SMAP-Reg soil moisture product is that it is fully consistent with the SMOS Level 3 soil moisture product, as the regression equations are calibrated based on SMOS Level 3 data (soil moisture and TB). Furthermore, the idea here is to re-build a coherent and consistent soil moisture data set rather than to develop a new algorithm or to surpass the well-established radiative transfer models (e.g. the L-band Microwave Emission of the Biosphere (L-MEB) model, LRPM, etc.).

To thi s end, two specific objectives of this study are listed below:

i.   produce a soil moisture product (SMAP_Reg) from SMAP TB that is consistent with SMOS soil moisture retrievals using physically-based regression equations; and

ii.   compare SMAP_Reg with operational SMAP and SMOS soil moisture retrievals against ground-based soil moisture measurements.

Since SMAP soil moisture products are relatively recent, their evaluation and their inter-comparison with other soil moisture data sets are required (Chan et al., 2016; Zeng et al., 2016). To advance our goal, therefore, the second objective of this study is two-fold: to evaluate the SMAP_Reg product, and to carry out a first evaluation of the agreement between SMAP and SMOS level 3 soil moisture products on global scale and against ground-based measurements (sparse and dense networks). The aim is not to establish which product is more accurate with respect to *in situ* but to understand the spatio-temporal patterns of SMAP relative to SMOS and how SMAP differs from SMOS globally. The agreement and degree of dispersion between the SMAP and SMOS soil moisture products are analyzed here in terms of four classical statistical criteria: Root Mean Squared Error (RMSE), Bias, Unbiased RMSE (UnbRMSE), and correlation coefficient (R) during the overlapping period (from Apr 2015 to Jul 2016).

The datasets, the local regression method, and the evaluation metrics used in this study are described in Section 2. Results are presented in Section 3. Finally, discussion and conclusions are provided in Section 4 and Section 5, respectively.

2. Materials and methods

2.1 Datasets

2.1.1 SMOS level 3 TB and soil moisture products—SMOS is a joint ESA, CNES (Centre national d'études spatiales), and CDTI (the Spanish government agency with responsibility for space) mission that was launched on November 2, 2009 (Kerr et al., 2012). The SMOS satellite carries an interferometric radiometer that operates at L-band, with multiple incidence angles, a spatial resolution of 35 km at the center of the field of view, a revisit time of 3 days, and ascending and descending overpass at 6:00 AM (local time) and 6:00 PM, respectively (Kerr et al., 2001; Kerr et al., 2010). Global SMOS Level 3 gridded multi-angular TB and soil moisture (top 0–5 cm surface layer) products (SMOSL3; version R04+OPER) are generated and provided by the CATDS (Centre Aval de Traitement des Données) center in France (Kerr et al., 2013). The SMOSL3 products are delivered for both orbits i.e. ascending and descending, projected on a global EASE (Equal Area Scalable

Earth) grid (V2) 25 km, by the CATDS, and are available online via http://www.catds.fr/. The IFS (Integrated Forecast System) soil temperature product from the European Centre for Medium-Range Weather Forecasts (ECMWF) is used in the SMOSL3 algorithm to retrieve the SMOSL3 soil moisture.

SMOSL3 TB product provides multi-angular TB data (in Kelvin) at the top of the atmosphere, i.e. *not* at the surface level and without correction for select reflected extraterrestrial sky (e.g., cosmic and galactic) and atmosphere contributions, but after projection onto the Earth reference frame (unlike the operational Level 2 product). The multi-angular TB are binned and averaged in 5°-width incidence angle bins with the center ranging from 2.5° to 62.5°. CATDS has recently provided SMOSL3 TB at 40°, and for this purpose the multi-angular TB are binned and averaged in 2°-width incidence angle bins. SMOSL3 soil moisture products (provided in m^3/m^3) are derived from the multiangular inversion of the L-MEB model (L-MEB algorithm) (Wigneron et al., 2007), i.e. the same method used for Level 2 soil moisture retrieval (Kerr et al., 2012), but are improved by using several revisits simultaneously (Kerr et al., 2016). SMOS TBs for ascending passes only and their associated soil moisture retrievals were used in this study (Al-Yaari et al., 2014a; Al-Yaari et al., 2014b) for a better consistency with SMAP soil moisture retrieval datasets, which are only provided at 6:00 AM.

Radio Frequency Interferences (RFI) originating from man-made emissions have been shown to affect the quality of the SMOS TB observations (Oliva et al., 2012). RFI probability is used to filter the SMOS datasets. This probability is the total number of deleted TBs due to suspected RFI on a certain period divided by the total number of TB measurements acquired during the same period available in the SMOS L1C datasets. In this study, SMOS TB and soil moisture data were excluded when the RFI probability is higher than 20% following Kerr et al. (2016). The reader is referred to the Algorithm Theoretical Based Document (Kerr et al., 2013) for more details on the SMOSL3 products.

2.1.2 SMAP level 3 TB and soil moisture products—SMAP is a NASA satellite that was launched on January 31, 2015. The SMAP satellite at launch carried two instruments: a Synthetic Aperture Radar and a radiometer operating at L-band, with a fixed incidence angle of 40°, a spatial resolution of 40 km, a revisit of 2–3 days and ascending and descending overpass at 6:00 PM (local time) and 6:00 AM, respectively (Entekhabi et al., 2010; Piepmeier et al., 2016). Soil moisture (top 0–5 cm surface layer) and freeze/thaw were supposed to be provided with three spatial resolutions ~3 km (high-resolution from radar), ~9 km (intermediate-resolution from radar and radiometer), and ~36 km (low-resolution from radiometer), projected on the EASE V2 grid. However, the radar instrument onboard SMAP satellite stopped transmitting data on Jul 7, 2015 due to a problem in the radar's high-power amplifier (Chan et al., 2016). Currently, soil moisture products are retrieved from SMAP TB radiometer data using the baseline Single Channel Algorithm (SCA) V-pol (Chan et al., 2016; Jackson, 1993). The global daily SMAP level 3 V3 gridded descending brightness temperature (at both H and V polarizations) and soil moisture (which is a compilation of 24 hrs of L2 soil moisture orbits) products, henceforth referred to here as SMAP_SCA, on EASE 2 grid (36 km) were used in this study. Unlike the SMOSL3 TBs product, the TBs provided within the SMAP L3 product are calibrated at the surface level,

i.e. corrected for Sky radiation and atmosphere contributions using auxiliary near surface information (De Lannoy et al., 2015). The SMAP L2 half-orbit soil moisture product (and also the SMAP L3 soil product) uses ancillary data (including soil temperature information) from the NASA's Global Modeling and Assimilation Office (GMAO/GEOS-5) Forward Processing product, which is provided with SMAP datasets. They are freely available from the National Snow and Ice Data Center (NSIDC). For more details on the SMAP mission and SMAP passive products, the reader is referred to (Chan et al., 2016; Piepmeier et al., 2016) and the SMAP Level 2 & 3 Soil Moisture (Passive) Algorithm Theoretical Basis Document (SMAP_ATBD) available here: https://nsidc.org/data/docs/daac/smap/sp_l2_smp/ pdfs/L2_SM_P_ATBD_v7_Sep2015-po-en.pdf.

Furthermore, it should be noted that both the SMOS and SMAP TB and soil moisture datasets were filtered prior to the regression analysis and the evaluations. A pixel was masked out when:

i. it is not considered as "Land" in the United States Geological Survey (USGS) Land-Sea mask (water fraction above 10%)";

ii. it is classified as "Urban and Built-Up", "Snow and Ice", "Water", "Permanent Wetlands", "Evergreen Needleleaf Forest", or "Evergreen Broadleaf Forest" according to the International Geosphere Biosphere Programme (IGBP) land cover map;

iii. the number of retrievals < 15 over the whole retrieval period;

iv. it corresponds to a date where the MERRA-Land soil temperature is < 274 K (to avoid frost and frozen conditions);

v. SMOS TB is estimated to be not sensitive to the surface effects according to the mask developed by Parrens et al. (2016); and

vi. it corresponds to a date that is not recommended for retrieval based on the SMAP quality flag.

2.1.3 MERRA-Land soil temperature—The soil temperature product was extracted from the NASA MERRA-Land product, which is a land-surface model forced with atmospheric reanalysis fields (precipitation corrected using gauges) (Reichle et al., 2011). MERRA_Land is a supplemental land surface data product of the Modern-Era Retrospective analysis for Research and Applications (MERRA) datasets, produced by the Goddard Earth Observing System model and assimilation system. MERRA-Land uses an updated catchment land surface model (version Fortuna-2.5) and includes a gauge-based precipitation data from the NOAA Climate Prediction Centre. The accuracy and precision of MERRA-Land soil temperature were assessed and analyzed by Parinussa et al. (2011) and Holmes et al. (2012). These studies found the performance of MERRA-Land to be similar to the ECMWF soil temperature products. The MERRA-Land product is available for the 1980-February 2016 period, provided with high temporal resolution (hourly) and a horizontal resolution of 2/3° longitude by 1/2° latitude (http://gmao.gsfc.nasa.gov/research/ merra/merra-land.php). The follow-up re-analysis product is MERRA2. It has improved soil temperature estimates, and uses gage information to correct the precipitation (Reichle et al.,

2016), similarly to (but not exactly the same as) MERRA-Land. At the time of writing, the MERRA2 product was not yet available. Consequently, this study uses MERRA-Land auxiliary information.

2.1.4 ECMWF soil temperature—The global atmospheric reanalysis ERA-Interim soil temperature datasets obtained from ECMWF were used in this study. The Hydrology-Tiled ECMWF Scheme for Surface Exchange over Land (H-TESSEL) is used by the ECMWF forecasts to solve for several parameters including a four-layer soil temperature profile (Balsamo et al., 2009). In this study, the soil temperature from the first layer (0–0.07 m) provided at 00:00, 06:00, 12:00, 18:00 UTC over a grid with a space sampling of 0.25×0.25 degrees was used. The ECMWF product is available from 1979 to present. The ECMWF datasets can be freely accessed at: http://apps.ecmwf.int/datasets/ and more information can be found in Berrisford et al. (2011).

2.1.5 Ground-based measurements—Validation of remotely sensed soil moisture products against ground-based measurements is a necessary step before any use. Nowadays several soil moisture networks share ground-based soil moisture measurements via the website of the International Soil Moisture Network (ISMN; Dorigo et al., 2011; Dorigo et al., 2015). ISMN is an ESA funded project initiated through the SMOS CAL/VAL. Data can be freely obtained from ISMN at https://ismn.geo.tuwien.ac.at/. All sites from ISMN that provide soil moisture within the period of Apr 2015–Jul 2016 were used in this study to evaluate the remotely sensed soil moisture products. Most of the sites are located in different regions with different vegetation, climate, and soil conditions.

Eleven networks in North America, Australia, Africa, and Europe were used namely: the PBO_H2O (http://xenon.colorado.edu/portal) network (Larson et al., 2008), the SCAN (Soil Climate Analysis Network) network (http://www.wcc.nrcs.usda.gov/scan/) (Schaefer et al., 2007), the SNOTEL (Snow Telemetry) network (http://www.wcc.nrcs.usda.gov/snow/), the USCRN (U.S. climate reference) network (Bell et al., 2013), the newly built RSMN (Romanian Soil Moisture & Temperature Observation Network) network (http://assimo.meteoromania.ro/) in Romania, the FMI (Finnish Meteorological Institute) network (Rautiainen et al., 2012) in Finland, the Oznet (Australian Moisture Monitoring Network) network (Smith et al., 2012) in Australia, the SMOSMANIA (Soil Moisture Observing System–Meteorological Automatic Network Integrated Application) network (Albergel et al., 2008; Calvet et al., 2007) in France, the DAHRA network (Tagesson et al., 2015) in Senegal, the iRON (Integrated Roaring Fork Observation Network) network http://ironagci.blogspot.co.at/, and the REMEDHUS (Soil Moisture Measurement Stations network of the University of Salamanca) network (Sanchez et al., 2012) in Spain. To ensure the high quality of the *in situ* measurements and to minimize the systematic differences between them and the remotely-sensed soil moisture products, we restricted the validation step to sites with a top soil layer of ~ 0 – 5 cm and with a minimum number of temporal 15 measurements. ISMN quality flags associated with the soil moisture data were applied (Dorigo et al., 2013). Consequently, ~ 400 (out of ~ 1000) sites from 11 networks were used for the evaluation. Moreover, if multiple sensors fall within one pixel, each sensor is treated independently: in this paper, unlike (De Lannoy & Reichle, 2015) we will not seek to

construct reliable statistical confidence intervals. Fig. 1 shows the locations of the different *in situ* soil moisture sites.

2.2 Methodology

The methodology used in this study to retrieve soil moisture from SMAP TB based on regression coefficients, obtained from SMOS TB and soil moisture, is schematized in Fig. 2. It consists of two steps: the calibration and the data production.

2.2.1 Calibration—A regression equation was analytically derived from the general (tau-omega) model equations (Mo et al., 1982) by Wigneron et al. (2004):

$$\ln (SM) = a_0 + a_1 \ln (\Gamma_H) + a_2 \ln (\Gamma_V) \quad (1)$$

Where a_0, a_1, and a_2 are regression coefficients, and the first (second) term on the right hand side of Eq. (1) represents the surface reflectivity at horizontal (vertical) polarization (Γ_P), described as:

$$\Gamma_P = 1 - \frac{T_{BP}}{T_G} \quad (2)$$

where:

T_{BP} is the brightness temperature at polarization p (H or V) at 40° incidence angle and T_G is the surface soil temperature.

We used a multiple linear regression i.e., a statistical technique that predicts the outcome of a response (dependent) variable using two or more independent (explanatory) variables. The coefficients of Eq. (1) were estimated using ordinary least squares techniques that minimize the sum of the squared errors. Eq. (1) was used in this study to retrieve soil moisture from the SMAP L-band TB observations. The coefficients a_0, a_1, and a_2 of Eq. (1) were calibrated per land cover category (obtained from the IGBP land cover map (see Fig. 1)) using the most recent available re-processed SMOS datasets: the SMOS TB in both V and H polarizations at incidence angle of 40° and soil moisture, and MERRA T_G datasets. The calibration was done during the 2013–2014 period. Note that this calibration was made here per land cover category, and not on a pixel to pixel basis as it was made previously in most LRM studies based on space-borne observations (Al-Yaari et al., 2016; Parrens et al., 2012; Saleh et al., 2006). This choice was made here to increase the spatial coverage. SMOS TBs observations are highly affected by RFI and therefore most of the regions in Europe and Asia would be masked out. To overcome this issue, we removed pixels with high RFIs and then we calibrated the regression equation with the rest of pixels within each land cover category. Lastly, we applied the obtained coefficients to the SMAP TB data (which are less impacted by RFI) for all the pixels for each land cover category.

2.2.2 Soil moisture production—Soil moisture was computed from the SMAP TB data for the Apr 2015 – Jul 2016 period using the regression coefficients computed in the calibration step using Eq. (1). This was done given the fact that we have all inputs for Eq. (1) to compute the soil moisture: TB observations at both polarizations from SMAP, T_G datasets based on the GMAO GEOS-5 (here in after referred to as GEOS-5) model provided with the SMAP datasets (or any other source like ECMWF), and the coefficients (a_0, a_1, and a_2) from the calibration step.

2.3 Metrics used for evaluating the soil moisture data set

The SMAP_Reg soil moisture product, obtained using the LRM algorithm, was compared with the SMAP and SMOS official Level 3 soil moisture products, and all three remotely sensed soil moisture products were evaluated against *in situ* observations. This was achieved using classical metrics: Root Mean Square Error (RMSE; m^3/m^3), Bias (m^3/m^3), UnbRMSE (m^3/m^3) (Entekhabi et al., 2010), and the (Pearson) correlation coefficient (R), which can be computed as follows:

$$Bias = \frac{1}{N} \sum_{i=1}^{N} S_i - O_i \quad (3)$$

$$RMSE = \sqrt{\frac{1}{N} \sum_{i=1}^{N} (S_i - O_i)^2} \quad (4)$$

$$UnbRMSE = \sqrt{RMSE^2 - bias^2} \quad (5)$$

$$R = \frac{1}{(N-1)} \sum_{i=1}^{N} \left(\frac{S_i - \bar{S}}{\sigma_S} \right) \left(\frac{O_i - \bar{O}}{\sigma_O} \right) \quad (6)$$

where the overbar indicates the mean;

- *Si* is the *i*th remotely sensed soil moisture value;

- *Oi* is the *i*th *in situ* observed or the remotely sensed soil moisture value;

- *N* is the total number of observations; and

- σ_o and σ_s are the standard deviations of the *in situ* observed or remotely sensed soil moisture values, respectively.

Moreover, Taylor diagrams (Taylor, 2001) were used in this study to compare in a comprehensive way the remotely sensed soil moisture and the *in situ* soil moisture measurements. Three statistics are summarized in a Taylor Diagram: the normalized

standard deviation (SDV) displayed as a radial distance, the correlation coefficient (R) displayed as an angle in the polar plot, and the centered RMSE (displayed as the distance to the point (observed) where R and SDV are equal to one). The performance of the remotely sensed soil moisture products is considered closest to ground measurements with the shortest distance to R = 1 and SDV = 1.

3 Results

3.1 SMAP and SMOS inter-comparison

Before presenting the regression analyses and evaluating the SMAP_Reg soil moisture product, it is necessary to evaluate and compare the measured (retrieved) Tb's (soil moisture) from SMOS and SMAP, which is the key to understand the different results, as it is the only input that changes between the SMAP and SMOS-based SM retrieval algorithms. For instance, this could help explain the differences in Bias, RMSE and correlation obtained between the different soil moisture products evaluated in this study over the different networks. For this purpose, global maps of R, RMSE, Bias, and UnbRMSE between SMAP and SMOS TBs and soil moisture were produced. Fig. 3 shows the global maps between SMOS and SMAP TBs during the Apr 2015 Jul 2016 period at both polarizations vertical (V-pol; left) and horizontal (H-pol; right): (a& e) correlation, (b& f) RMSE, (c& g) Bias, and (d &h) UnbRMSE. In general, there is a good agreement between SMOS and SMAP TBs at both V-pol and H-pol particularly in terms of temporal dynamics (R mostly > 0.8). The RMSE and UnbRMSE values are lower between SMAP and SMOS at V-pol than between SMAP and SMOS at H-pol over some regions (e.g., region of western North Africa). The RMSE (UnbRMSE) values range mostly between 2 and 8 (4) K over most of the globe except over some regions (e.g., Western Europe). SMAP presents cold (warm) bias with respect to SMOS over most of the globe (high latitude regions).

Fig. 4 displays global inter-comparison between the operational SMOS (L3) and SMAP (SCA) soil moisture retrievals during the Apr 2015–Jul 2016 period: (a) correlation, (b) RMSE, (c) Bias, and (d) UnbRMSE. The correlations between SMOS and SMAP soil moisture retrievals (Fig. 4a) are very high (between 0.8 and 1) over Australia, central Asia and USA, and the Sahel, while moderate and low correlations are found over the other regions. SMAP is much wetter under regions where the vegetation is moderate or high as well as on coastlines, whereas SMOS is wetter over India and Central America, and far north (see Fig. 4c). It can be seen in Figs. 4(b& d) that higher values of RMSE and UnbRMSE are found in regions where the vegetation is moderate or high than over arid and semi-arid regions. The retrieved soil moisture data from both SMOS and SMAP seem to agree generally well in terms of unbRMSE (mostly < 0.05 m^3/m^3).

3.2 Regression calibration

The regression coefficients a_0 (intercept coefficient), a_1 (coefficient for the H polarized TB), and a_2 (coefficient for the V polarized TB) in Eq. (1), obtained using SMOSL3 TB (V & H) and soil moisture in the calibration step, are presented in Table 1 and Fig. 5. A unique coefficient value for each land cover category was obtained. It can be seen that the values of the coefficient for the different land cover categories can be clearly distinguished. For

instance, lowest coefficients values for a_0 and a_2 were obtained over "Closed shrublands" and highest over "Deciduous needleleaf forest" for a_2 and "Deciduous broadleaf forest" for a_0 while lowest values for a_1 were obtained over "Cropland/Natural vegetation mosaic" and highest over "Deciduous broadleaf forest".

In order to make a first evaluation of the quality of the calibration step, and before applying the LRM algorithm to the SMAP TB data, we applied the LRM equations to the SMOS TB data. The soil moisture product (SMOS_Reg) was retrieved from SMOSL3 TB using the regression coefficients computed from Eq. (1) over the calibration period. Then, SMOS_Reg was compared with the reference SMOSL3 soil moisture for the same period in terms of RMSE and correlation coefficient (P-value < 0.05).

Looking at the correlation map in Fig. 6a, a remarkable agreement (R > 0.8) can be seen between SMOS_Reg and SMOSL3 over most of the globe except over some forests areas (e.g., boreal regions) where the correlation values drop below 0.4. Looking at the RMSE map in Fig. 6b, the spatial patterns of the RMSE values are also found to be in correspondence with the vegetation distribution: low RMSE values (~ 0.05 m^3/m^3) are found over areas with low vegetation while high RMSE values are found over moderately vegetated regions.

3.3 SMAP_Reg soil moisture evaluation

This section presents an evaluation of the SMAP_Reg soil moisture product, which was based on applying the LRM algorithm to the SMAP Level 3 TB observations (see Section 2.2.2) and using two soil temperature products: GEOS-5 and ECMWF. Note that the LRM algorithm was calibrated with MERRA-Land soil temperature; here, we only change the input, not the linear regression coefficients, as it will become clear that the temperatures estimated in GEOS-5 and ECMWF do not differ much in the first order. Both these SMAP_Reg soil moisture products were first compared with the SMAP operational Level 3 soil moisture product (SMAP_SCA) to investigate the similarity/dissimilarity between the various SMAP soil moisture products. This was done by computing the R and RMSE statistical criteria between the SMAP_Reg and SMAP_SCA soil moisture products at the global scale. The temporal correlation between SMAP_Reg and SMAP_SCA soil moisture retrievals is shown in Fig. 7a using GEOS-5 and in Fig. 7c using ECMWF. Figs. 7a & c show that the temporal dynamics of both SMAP_Reg and SMAP_SCA soil moisture products are generally very similar with R values larger than 0.8 over most of the globe. However, weaker correlations between SMAP_Reg (ECMWF) and SMAP_SCA (GEOS-5) than between SMAP_Reg (GEOS-5) and SMAP_SCA (GEOS-5) can be seen over a few regions particularly over high latitude areas and Sahara. Fig. 7b shows that the distribution of the RMSE values between SMAP_Reg and SMAP_SCA soil moisture products present clear spatial patterns: low RMSE values over deserts and savannahs (e.g., the Sahara, Australia, Southern Africa, etc.), whereas high values of RMSE values were generally found over vegetated areas. Looking at both Figs. 7a &c (correlations) and Figs. 7b &d (RMSE), there is a general good agreement between SMAP_Reg and SMAP_SCA over regions with low to moderate amounts of vegetation cover.

The SMAP_Reg soil moisture product with GEOS-5 soil temperature as auxiliary input was additionally evaluated against

    i. *in situ* soil moisture observations using more than 400 sites from eleven networks spread over the globe (see Section 2.1.4); and

    ii. the operational SMAP and SMOS Level 3 soil moisture products at these individual site locations. The SMAP_SCA and the SMOSL3 soil moisture products were considered in the evaluation in order to investigate the consistency in time variations between the new soil moisture product (SMAP_Reg) and the original ones at different sites.

Taylor diagrams (see Section 2.2.3) given in Fig. 8 show the statistics for the sites individually. Fig. 8 shows values of SDV, R, and the centered RMSE between the remotely sensed soil moisture products and measured soil moisture values over all sites used in this study. In Fig. 8, the performance of SMAP_SCA (blue symbols), SMAP_Reg (red symbols), and SMOSL3 (green symbols) varies from one site to another and from one network to another as demonstrated by the uneven distribution of the sites (shown as circles) in the plots. Looking at the Taylor diagram over the SCAN and SNOTEL sites, the correlations values range between 0 and 0.9 and both SMAP_Reg and SMOSL3 tend to have higher SDV values than SMAP_SCA. Over the REMEDHUS sites, the three algorithms have a comparable performance but with a large variability (as defined by high SDV index) with the *in situ* observations; the correlation values range between 0.4 and 0.8. Over the PBO-H2O sites, SMAP_SCA patterns are closer to the *in situ* patterns than SMOSL3 and SMAP_Reg, which have larger SDV values than the *in situ* observations and most of the correlation values range between 0.5 and 0.9. Over the USCRN sites, the retrieved soil moisture values from all algorithms have a similar variability to that of the *in situ* observations, although SMAP_Reg and SMOSL3 soil moisture products have a larger variability for some sites. Over the RSMN sites, the three products present the same level of performance with respect to the *in situ* observations but all had higher SDV than the *in situ* observations. However, the correlations drop below 0.4 for a few sites for the three products. Over the DAHRA network, the SMOSL3 (best correlation) and SMAP_SCA product lie closest to the observed point followed by SMAP_Reg with higher SDV than the *in situ* observations for all products. Over the iRON sites, the correlations range from 0.4 to 0.8 for the SMOSL3 and SMAP_Reg. SMAP_SCA and SMAP_Reg are comparable in terms of variability and they are closer to the *in situ* patterns than SMOSL3. Over the Oznet network, the three products are comparable in terms of correlations (ranging from 0.6 to 0.9) and, similarly to the RSMN network, overestimate the *in situ* observations. Over the FMI sites, the correlations range from 0.4 to 0.8 and 0.9 for SMAP_SCA and SMAP_Reg, respectively. Similarly, to what was obtained over the Oznet sites, the SMAP_SCA and SMAP_Reg products overestimate the *in situ* observations over most of the sites. Finally, over SMOSMANIA, SMAP_Reg has better correlations, with *in situ* data ranging from 0.4 to 0.95, than the other two products. For SMOSL3, the correlations drop below 0.4 for a few sites. Overall, all three products have approximately the same level of performance in terms of variability but SMAP_SCA is slightly better in terms of temporal dynamics.

In order to have a general idea on the overall performance of SMAP_SCA, SMAP_Reg, and SMOSL3, the average of the Bias, RMSE, and UnbRMSE values and the median of the correlation values for all sites were computed per each network. Given the different sizes of the networks, the varying sample sizes, and varying temporal and spatial autocorrelations, the values are only indicative and no statistical confidence levels are provided. It should be noted that the average and median values were only computed when the site has a number of observations > 15 and p-value <0.05. This is presented in Table 2 and Fig. 9, which show the comparison statistics for the three algorithms i.e. SMAP_Reg, SMAP_SCA, and SMOSL3 against the *in situ* observations. It can be seen in Table 2 and Fig. 9 that the best R scores (R > 0.80) for the three algorithms were obtained over the Oznet sites while the worst ones were observed over (R ~ 0.58) over the SNOTEL sites for SMAP_SCA and over the DAHRA and SMOSMANIA sites (R=0.51 and R=0.45 for SMAP_Reg and SMOSL3 respectively). SMOSL3 had highest R values over the DAHRA site while SMAP_Reg had highest R values over SMOSMANIA. Other than those two networks, SMAP_SCA had highest R values. However, both SMAP products i.e. SMAP_SCA and SMAP_Reg have comparable performance particularly in terms of correlation coefficients. In terms of unbRMSE, SMAP_SCA had lower values for all sites except in Oznet where the lowest values were obtained by SMOSL3. Even though it is difficult to compare absolute values at *in situ* locations, a comparison based on a large sample can give some indication of biases: the Bias values showed that all products are generally dry, except over RSMN, DAHRA, and Oznet (and FMI for SMAP_SCA). Unlike SMAP_Reg, a notable overall positive bias is obtained over FMI for SMAP_SCA (overestimation). The overestimation of *in situ* soil moisture observations over RSMN and FMI networks by SMAP_SCA is in line with the recent findings of Zeng et al. (2016).

4 Discussion

We investigated the potential utility of a physically based multi-linear regression approach to retrieve soil moisture from two microwave remote sensing satellites that operate at L-band: SMOS and SMAP. The approach consists of two steps:

   i.   a calibration step to compute regression coefficients using SMOS TB and soil moisture over 2013–2014 (calibration period); and

   ii.   a production step to retrieve soil moisture from SMAP TB using the computed regression coefficients, for Apr 2015 to Jul 2016 (production period).

4.1 SMAP and SMOS inter-comparison

Before applying the regressions, an inter-comparison was made between SMOS and SMAP TBs and soil moisture. From the results (Fig. 3 & 4), it was shown that there is a very good agreement between the two datasets. However, small discrepancies (2 to 4 K of Bias) between the SMOS and SMAP TBs were found over most of the globe and high discrepancies were found particularly over regions affected by RFI (Western Europe, North Africa, etc.). This is not unexpected due to the fact that, as indicated in Section 2.1.1 and 2.1.2, the SMOSL3 TB product provides TBs on top of the atmosphere and there is no correction for sky and atmosphere contributions whereas SMAP TB is provided at the

surface. According to De Lannoy et al. (2015), a difference of less than 2 K for H-Pol TB and 1 K for V-Pol TB at 40° incidence angle between SMOS TB and SMAP TB can be attributed to the contributions of the atmospheric and reflected sky (e.g., cosmic and galactic) radiations. This low difference can be explained by the fact that the effects of (i) the contribution of the atmosphere to TB (direct and reflected) and (ii) the attenuation effects due to the atmosphere, partially offset each other. Nevertheless, local and short-term values regularly exceed 5 K (De Lannoy et al., 2015). In addition, SMAP TBs are water-body corrected while SMOS TBs are not. Thus, the SMOS and SMAP TBs do not correspond exactly to the same pixel coverage: the SMOS TBs correspond to the whole pixel, while the SMAP TBs correspond to the whole pixel, but excluding open water areas. As the emission of open water surfaces (~ 60 – 150 k) is small in comparison to the emission of soil and vegetation-covered surfaces, applying this correction leads systematically to an increase in the TBs values. Note that for pixels with a fraction of water bodies higher than 10%, data were filtered out. But even after this filtering, the water TB correction may have an impact on the TB values. This water TB correction may explain the warm "Bias" (~10 K) of the SMAP TBs with respect to the SMOS TBs over high latitude and boreal regions (where many pixels may contain lakes, rivers, wetlands, etc.). Excluding these regions, a small cold bias of SMAP TBs with respect to SMOS TBs can be noted (~3–6 K). Overall, a very good agreement was found globally between the SMAP and SMOS TBs data.

4.2 Regression calibration and soil moisture production

The regression model was run for each land cover category (defined here using the IGBP land cover map) separately and thus we obtained coefficients of each land cover category. These values vary from one land cover category to another, reflecting the different characteristics for each land cover category. These three parameters as indicated by Saleh et al. (2006) are a function of the soil type and roughness. The regression approach quality was evaluated in two ways:

  i.   first, we estimated soil moisture from SMOS TB and compared the predicted soil moisture (SMOS_Reg) to the reference (SMOSL3) using correlation and RMSE, over the calibration period (2013–2014). High correlations (R> 0.8) and low RMSE values were obtained between SMOS_Reg and the reference over the continental surfaces, indicating that the spatio-temporal dynamics of SMOSL3 was well captured by SMOS_Reg. However, some differences can be noted in terms of magnitude over high to moderate vegetation areas and high latitude regions. This is not unexpected due to uncertainties in the SMOS datasets caused by the high vegetation attenuation effects in these regions, which is a major problem for most of the remotely sensed soil moisture retrievals (Vittucci et al., 2016; Wigneron et al., 2003); and

  ii.   Second, we estimated soil moisture from SMAP TB for the Apr 2015 to Jul 2016 period (SMAP-Reg) and compared it to the original SMAP_SCA and the SMOSL3 soil moisture products against more than 400 sites over the world.

Soil temperature is an important input in the radiative transfer equation and has a significant impact on the final estimate of the soil moisture retrievals (Holmes et al., 2012; Lv et al., 2016; Parinussa et al., 2011). In order to study how sensitive is the retrieved soil moisture to

the soil temperature effects, we used soil temperature from two different sources: ECMWF and GEOS-5. We applied the regression coefficients to SMAP TB using these two products and then we compared with SMAP_SCA. It was found that in general the spatial patterns are similar for both products in terms of R and RMSE values; however, the correlations between SMAP_Reg (ECMWF) and SMAP_SCA (GEOS-5) are lower than the correlations between SMAP_Reg (GEOS-5) and SMAP_SCA (GEOS-5) over some regions (e.g., Sahara, Far Eastern Federal District, East-Central Canada, etc.). The better agreement between SMAP_Reg (GEOS-5) and SMAP_SCA (GEOS-5) does not necessarily mean that the quality of GEOS-5 is better than ECMWF. This could simply results from the fact that the same soil temperature product was used in both the regression approach and the SMAP_SCA algorithm. However, it does seem that soil temperature has an important impact on the soil moisture retrievals (e.g., Lv et al., 2016), i.e. using the same soil temperature leads to similar soil moisture retrievals from SMAP no matter if different retrieval approaches are used. This could partially explain the strong agreement found between SMAP_SCA and SMAP_Reg.

Results from the comparison between SMAP_Reg both (ECMWF & GEOS-5) and SMAP_SCA showed that SMAP_Reg is in agreement with SMAP_SCA, particularly in terms of temporal dynamics which is of high relevance (Crow et al., 2010; Liu et al., 2012). Moreover, it is noticed here that the performance of the "production" step i.e. comparison between SMAP_Reg and SMAP_SCA is much better than the "calibration" step i.e. comparison between SMOS_Reg and SMOSL3. This can be partly explained by three reasons:

1.   in the calibration step, the TBs used are not exactly the same while in the production step they are. More specifically, the SMOSL3 soil moisture product is not directly retrieved from SMOSL3 TB but from TB products in the Fourier domain (L1B); thus the TB used in the regression does not necessarily match the actual TB used to retrieve SMOSL3 soil moisture. Therefore it is expected that the temporal dynamics of the two soil moisture products will be more similar because they will be driven by the common input TB dynamics. This uncertainty, among others, may affect the quality of the calibration;

2.   the quality of SMAP TB seems to be very good and therefore whatever the used algorithm, the resultant soil moisture is the same particularly in terms of temporal dynamics. This, again, may partially explain the strong similarity between the two products i.e. SMAP_Reg and SMAP_SCA; and

3.   the regression (LRM coefficients) is based on MERRA-Land T_G, which is similar to the GEOS-5 product used in SMAP_SCA and not in SMOSL3 (for which the ECMWF product is used); explicitly indicating that soil temperature may play a crucial role in the quality of the SM retrievals.

4.3 SMAP_Reg soil moisture evaluation

Results from evaluating both SMAP products and SMOSL3 against *in situ* observations showed that SMAP_SCA and SMAP_Reg soil moisture products have comparable performance with similar R values over the REMEDHUS, PBO_H2O, SNOTEL, SCAN,

Oznet, and USCRN sites. Nevertheless, all three remotely sensed soil moisture products had poor performance over the SNOTEL. The poor performance of the three algorithms over the SNOTEL network can be attributed to several reasons: among them it should be considered that most of the SNOTEL sites are located in mountain regions with forests and freezing and thawing processes, more details on these aspects can be found in Al Bitar et al. (2012). It should be kept in mind that when using only the recommended retrievals for SMAP, there was no data left from the iRON sites. So the statistics for this particular network were based on data without considering if the retrieval was recommended or not but other filters were, however, applied.

All remotely sensed soil moisture products underestimated generally the *in situ* observations used in this study. The bias values ranged from –0.095 m^3/m^3 (SMOSMANIA) to 0.066 m^3/m^3 (DAHRA) for SMAP_Reg, from –0.094 m^3/m^3 (iRON) to 0.076 m^3/m^3 (FMI) for SMAP_SCA, and from –0.182 m^3/m^3 (iRON) to 0.026 m^3/m^3 (RSMN) for SMOSL3. This so-called "dry" bias of SMOSL3 and SMAP_SCA is in line with previous studies (Al-Yaari et al., 2014b; Al Bitar et al., 2012; Chan et al., 2016; Dente et al., 2012). On the other hand, an overestimation was found over FMI (for only SMAP_SCA) and RSMN, DAHRA, and Oznet sites (for the three products). It should be kept in mind that FMI is a very specific network: the sites of FMI are located in high latitude regions with cold climate in which remotely-send soil moisture retrievals are influenced by the effects of soil freezing and thawing processes, organic matter in the soil substrate and the presence of numerous water bodies and bogs (Rautiainen et al., 2012; Zeng et al., 2016). The reasoning behind the underestimation/overestimation of the *in situ* soil moisture values is a challenge. The dry bias could be related to the different spatial scales and sampling depths between the satellites and the *in situ* observations (e.g., Dorigo et al., 2015; Escorihuela et al., 2010; Rondinelli et al., 2015). Moreover, although RFI was severely filtered from the SMOS datasets, it could be that some sources of RFI are still not filtered/detected, which can explain the rather general underestimation which is found in this study (Oliva et al., 2016). This was evident especially for SMOS as seen in Fig. 3 where SMOS still has higher TBs close to those regions despite filtering RFI. The reader is referred to Al Bitar et al. (2012) for a discussion on these questions.

In terms of UnbRMSE, a comparable performance between SMAP_SCA and SMAP_Reg was found over the SMOSMANIA, iRON, and SNOTEL sites but lower values were obtained with SMAP_SCA over the other networks. SMOSL3 had generally higher UnbRMSE values than both SMAP_SCA and SMAP_Reg. However, SMOSL3 had lower values over the Oznet and DAHRA sites.

It was noted from Table 2 and Fig. 9, that the SMAP TB-based soil moisture products (SMAP_SCA and SMAP_Reg) have a slightly better performance than SMOSL3 for most of the networks especially in terms of temporal dynamics. Although the three algorithms use TB at L-band and rely on the same radiative transfer equation (tau-omega model), they vary in many things (e.g., ancillary datasets, model parameterizations and assumptions). For instance, SMOS and SMAP use two different land cover maps: ECOCLIMAP 2004 (containing 213 classes) for SMOS and MODIS IGBP (containing 17 classes) for SMAP, so it is likely there is a mismatch between the real land cover and the theoretical land cover

used in SMAP and SMOS soil moisture retrievals leading to a different behavior of the soil moisture retrievals. This may also partially explain the similarity between SMAP_Reg and SMAP_SCA given the use of the same land cover. These differences were already noted in the direct intercomparison between SMOSL3 and SMAP_SCA displayed in Fig. 4. The SMOS team is currently investigating the impact of land cover mapping and the possibility to replace the ECOCLIMAP map by the IGBP map in the SMOS soil moisture retrieval algorithm. Furthermore, the better performance of SMAP soil moisture products could be related to the enhanced quality of the SMAP TB observations due to an improved RFI mitigation and detection system (Piepmeier et al., 2016). Moreover, SMOS TB observations have a radiometric error of ~ 3 to 3.5 K while SMAP TB observations have a radiometric error of ~ 1 K (De Lannoy et al., 2015). Finally, SMOS and SMAP use different surface soil temperature sources for their operational products.

Based on the presented results, it can be noted that applying regression analysis to TB (from SMAP and SMOS) observed at L-band (1.4 GHz) gave better results compared to what was found by Al-Yaari et al. (2016), who applied the LRM algorithm to TB observed at C-band (from AMSR-E; 6.9 GHz). This is not unexpected, as the simplifications and assumptions (e.g., neglecting the scattering effects) of the LRM method are more valid at L-band. Moreover, both SMAP and SMOS observe TB at the same frequency i.e. L-band, which is considered optimal for soil moisture retrievals (Chan et al., 2016; Jackson, 1993). On the other hand, a similar behavior with Al-Yaari et al. (2016) of the regression coefficients that correspond to the H polarization and V polarization was found: low (high) coefficient values at H polarization correspond generally to high (low) values at V polarization over most of the regions.

5 Conclusions

This study demonstrated the potential benefits of combining SMOS and SMAP datasets given the good performance of SMAP_Reg compared to SMOSL3 and SMAP_SCA original products over some regions. This in return shows the close similarity between SMOS and SMAP TB observations and highlights that an integration of SMAP and SMOS data sets to build a long term soil moisture record will be successful and higher temporal frequency. Finally, this first evaluation of preliminary SMAP products, and the inter-comparison with SMOS datasets provided insights and statistics that can be useful for SMAP/SMOS soil moisture product validation and SMAP/SMOS algorithm refinements and convergence on auxiliary data sets. A calibration of the soil and vegetation effects has been recently made (Fernández Morán et al., 2016). A new SMOS Level 3 soil moisture product integrating this new calibration and with a significantly improved accuracy is being produced. Future research will consider the calibration of SMAP-Reg with this new SMOS product and further fusion studies will be continued by applying LRM to the SMOS and SMAP datasets considering other important variables such as the vegetation opacity.

Acknowledgments

References

Aires F, Aznay O, Prigent C, Paul M, Bernardo F. Synergistic multi-wavelength remote sensing versus a posteriori combination of retrieved products: Application for the retrieval of atmospheric profiles using MetOp-A. Journal of Geophysical Research: Atmospheres. 2012:117.

Al-Yaari A, Wigneron JP, Ducharne A, Kerr YH, Wagner W, De Lannoy G, Reichle R, Al Bitar A, Dorigo W, Richaume P, Mialon A. Global-scale comparison of passive (SMOS) and active (ASCAT) satellite based microwave soil moisture retrievals with soil moisture simulations (MERRA-Land). Remote Sensing of Environment. 2014a; 152:614–626.

Al-Yaari A, Wigneron JP, Ducharne A, Kerr Y, de Rosnay P, de Jeu R, Govind A, Al Bitar A, Albergel C, Muñoz-Sabater J, Richaume P, Mialon A. Global-scale evaluation of two satellite-based passive microwave soil moisture datasets (SMOS and AMSR-E) with respect to Land Data Assimilation System estimates. Remote Sensing of Environment. 2014b; 149:181–195.

Al-Yaari A, Wigneron JP, Kerr Y, de Jeu R, Rodriguez-Fernandez N, van der Schalie R, Al Bitar A, Mialon A, Richaume P, Dolman A, Ducharne A. Testing regression equations to derive long-term global soil moisture datasets from passive microwave observations. Remote Sensing of Environment. 2016; 180:453–464.

Al Bitar A, Leroux D, Kerr YH, Merlin O, Richaume P, Sahoo A, Wood EF. Evaluation of SMOS Soil Moisture Products Over Continental U.S. Using the SCAN/SNOTEL Network. IEEE Transactions on Geoscience and Remote Sensing. 2012; 50:1572–1586.

Albergel C, Rüdiger C, Pellarin T, Calvet JC, Fritz N, Froissard F, Suquia D, Petitpa A, Piguet B, Martin E. From near-surface to root-zone soil moisture using an exponential filter: an assessment of the method based on in-situ observations and model simulations. Hydrology and Earth System Sciences Discussions. 2008; 12:1323–1337.

Balsamo G, Viterbo P, Beljaars ACM, van den Hurk BJJM, Hirschi M, Betts AK, KS. A revised hydrology for the ECMWF model: Verification from field site to terrestrial water storage and impact in the ECMWF-IFS. J Hydrometeor. 2009:10.

Bartalis, Z., Hasenauer, S., Naeimi, V., Wagner, W. ASCAT Soil Moisture Report Series, No. 14. Institute of Photogrammetry and Remote Sensing, Vienna University of Technology; Austria: 2007. WARP-NRT 2.0 Reference Manual.

Bell JE, Palecki MA, Baker CB, Collins WG, Lawrimore JH, Leeper RD, Hall ME, Kochendorfer J, Meyers TP, Wilson T, Diamond HJ. U.S. Climate Reference Network Soil Moisture and Temperature Observations. Journal of Hydrometeorology. 2013; 14:977–988.

Berg A, Lintner BR, Findell KL, Malyshev S, Loikith PC, Gentine P. Impact of Soil Moisture–Atmosphere Interactions on Surface Temperature Distribution. Journal of Climate. 2014; 27:7976–7993.

Berrisford, P., Dee, D., Poli, P., Brugge, R., Fielding, K., Fuentes, M., Kallberg, P., Kobayashi, S., Uppala, S., Simmons, A. ERA Report Series 1. ECMWF, Shinfield Park; Reading, UK: 2011. The ERA-Interim archive Version 2.0; p. 13177

Calvet, J-C., Fritz, N., Froissard, F., Suquia, D., Petitpa, A., Piguet, B. In situ soil moisture observations for the CAL/VAL of SMOS: The SMOSMANIA network. Geoscience and Remote Sensing Symposium, 2007. IGARSS 2007. IEEE International; IEEE; 2007. p. 1196-1199.

Chan S, Bindlish Rajat, O'Neill Peggy, Njoku Eni, Jackson Tom, Colliander Andreas, Chen Fan, Burgin Mariko, Dunbar Scott, Piepmeier Jeffrey, Yueh Simon, Entekhabi Dara, Cosh Michael H, Caldwell Todd, Walker Jeffrey, Wu Xiaoling, Berg Aaron, Rowlandson Tracy, Pacheco Anna, McNairn Heather, Thibeault Marc, Martínez-Fernández José, González-Zamora Ángel, Seyfried Mark, Bosch David, Starks Patrick, Goodrich David, Prueger John, Palecki Michael, Small Eric E, Zreda Marek, Calvet Jean-Christophe, Crow Wade T, Kerr Y. Assessment of the SMAP Passive Soil Moisture Product. IEEE Transactions on Geoscience and Remote Sensing. 2016; 54:4994–5007.

Chen T, McVicar RT, Wang G, Chen X, de Jeu AR, Liu YY, Shen H, Zhang F, Dolman JA. Advantages of Using Microwave Satellite Soil Moisture over Gridded Precipitation Products and Land Surface

Model Output in Assessing Regional Vegetation Water Availability and Growth Dynamics for a Lateral Inflow Receiving Landscape. Remote Sensing. 2016:8.

Choudhury BJ, Schmugge TJ, Chang A, Newton RW. Effect of surface roughness on the microwave emission from soils. Journal of Geophysical Research: Oceans. 1979; 84:5699–5706.

Crow WT, Miralles DG, Cosh MH. A Quasi-Global Evaluation System for Satellite-Based Surface Soil Moisture Retrievals. IEEE Transactions on Geoscience and Remote Sensing. 2010; 48:2516–2527.

De Lannoy GJM, Reichle RH, Peng J, Kerr Y, Castro R, Kim EJ, Liu Q. Converting Between SMOS and SMAP Level-1 Brightness Temperature Observations Over Nonfrozen Land. IEEE Geoscience and remote sensing letters. 2015; 12:1908–1912.

De Lannoy GJM, Reichle RH. Global Assimilation of Multiangle and Multipolarization SMOS Brightness Temperature Observations into the GEOS-5 Catchment Land Surface Model for Soil Moisture Estimation. Journal of Hydrometeorology. 2015; 17:669–691.

Dente L, Su Z, Wen J. Validation of SMOS Soil Moisture Products over the Maqu and Twente Regions. Sensors. 2012; 12:9965–9986. [PubMed: 23112582]

Dorigo WA, Wagner W, Hohensinn R, Hahn S, Paulik C, Xaver A, Gruber A, Drusch M, Mecklenburg S, van Oevelen P, Robock A, Jackson T. The International Soil Moisture Network: a data hosting facility for global in situ soil moisture measurements. Hydrol Earth Syst Sci. 2011; 15:1675–1698.

Dorigo WA, Xaver A, Vreugdenhil M, Gruber A, Hegyiová A, Sanchis-Dufau AD, Zamojski D, Cordes C, Wagner W, Drusch M. Global Automated Quality Control of In Situ Soil Moisture Data from the International Soil Moisture Network. Vadose Zone Journal. 2013:12.

Dorigo WA, Gruber A, De Jeu RAM, Wagner W, Stacke T, Loew A, Albergel C, Brocca L, Chung D, Parinussa RM, Kidd R. Evaluation of the ESA CCI soil moisture product using ground-based observations. Remote Sensing of Environment. 2015; 162:380–395.

Enenkel M, Reimer C, Dorigo W, Wagner W, Pfeil I, Parinussa R, De Jeu R. Combining satellite observations to develop a daily global soil moisture product for a wide range of applications. Hydrol Earth Syst Sci Discuss. 2015; 2015:11549–11589.

Entekhabi D, Njoku EG, O'Neill PE, Kellogg KH, Crow WT, Edelstein WN, Entin JK, Goodman SD, Jackson TJ, Johnson J, Kimball J, Piepmeier JR, Koster RD, Martin N, McDonald KC, Moghaddam M, Moran S, Reichle R, Shi JC, Spencer MW, Thurman SW, Leung T, Van Zyl J. The Soil Moisture Active Passive (SMAP) Mission. Proceedings of the IEEE. 2010; 98:704–716.

Escorihuela MJ, Chanzy A, Wigneron JP, Kerr YH. Effective soil moisture sampling depth of L-band radiometry: A case study. Remote Sensing of Environment. 2010; 114:995–1001.

Fernández Morán, R., Wigneron, J-P., De Lannoy, G., Lopez-Baeza, E., Mialon, A., Mamoodi, A., Parrens, M., Al Bitar, A., Richaume, P., Kerr, Y. Calibrating the effective scattering albedo in the SMOS algorithm: some first results. 2016 IEEE International Geoscience and Remote Sensing Symposium (IGARSS); Beijing. 2016; 2016.

Friedl MA, Sulla-Menashe D, Tan B, Schneider A, Ramankutty N, Sibley A, Huang X. MODIS Collection 5 global land cover: Algorithm refinements and characterization of new datasets. Remote Sensing of Environment. 2010; 114:168–182.

GCOS. Implementation Plan for the Global Observing System for Climate in Support of the UNFCC (2010 Update). 2010

Grant JP, Saleh-Contell K, Wigneron JP, Guglielmetti M, Kerr YH, Schwank M, Skou N, Griend AAVd. Calibration of the L-MEB Model Over a Coniferous and a Deciduous Forest. IEEE Transactions on Geoscience and Remote Sensing. 2008; 46:808–818.

Hirschi M, Mueller B, Dorigo W, Seneviratne SI. Using remotely sensed soil moisture for land–atmosphere coupling diagnostics: The role of surface vs. root-zone soil moisture variability. Remote Sensing of Environment. 2014; 154:246–252.

Holmes TRH, de Rosnay P, de Jeu R, Wigneron RJP, Kerr Y, Calvet JC, Escorihuela MJ, Saleh K, Lemaître F. A new parameterization of the effective temperature for L band radiometry. Geophysical Research Letters. 2006:33.

Holmes TRH, Jackson TJ, Reichle RH, Basara JB. An assessment of surface soil temperature products from numerical weather prediction models using ground-based measurements. Water Resources Research. 2012:48.

Hupet F, Vanclooster M. Intraseasonal dynamics of soil moisture variability within a small agricultural maize cropped field. Journal of Hydrology. 2002; 261:86–101.

Jackson TJ, Schmugge TJ. Vegetation effects on the microwave emission of soils. Remote Sensing of Environment. 1991; 36:203–212.

Jackson TJ. Measuring surface soil moisture using passive microwave remote sensing. Hydrol Process. 1993; 7:139–152.

Jackson, TJ., O'Neill, P., Njoku, E., SC, Bindlish, R., Colliander, A., Chen, F., Burgin, M., Dunbar, S., Piepmeier, J., Cosh, M., Caldwell, T., Walker, J., Wu, X., Berg, A., Rowlandson, T., Pacheco, A., McNairn, H., Thibeault, M., Martínez-Fernández, J., González-Zamora, Á., Seyfried, M., Bosch, D., Starks, P., Goodrich, D., Prueger, J., Su, Z., van der Velde, R., Asanuma, J., Palecki, M., Small, E., Zreda, M., Calvet, J., Crow, W., Kerr, Y., Yueh, S., Entekhabi, D. SMAP Project, JPL D-93720. Jet Propulsion Laboratory; Pasadena, CA: 2016. Soil Moisture Active Passive (SMAP) Project Calibration and Validation for the L2/3_SM_P Version 3 Data Products.

Kerr Y. Soil moisture from space: Where are we? Hydrogeology Journal. 2007; 15:117–120.

Kerr Y, Jacquette E, Al Bitar A, Cabot F, Mialon A, Richaume P, Quesney A, Berthon L, Wigneron J. The CATDS SMOS L3 soil moisture retrieval processor, Algorithm Theoretical Baseline Document (ATBD). SO-TN-CBSA-GS-0029. 2013

Kerr YH, Waldteufel P, Wigneron JP, Martinuzzi J, Font J, Berger M. Soil moisture retrieval from space: the Soil Moisture and Ocean Salinity (SMOS) mission. IEEE Transactions on Geoscience and Remote Sensing. 2001; 39:1729–1735.

Kerr YH, Waldteufel P, Wigneron JP, Delwart S, Cabot F, Boutin J, Escorihuela MJ, Font J, Reul N, Gruhier C, Juglea SE, Drinkwater MR, Hahne A, Martin-Neira M, Mecklenburg S. The SMOS Mission: New Tool for Monitoring Key Elements ofthe Global Water Cycle. Proceedings of the IEEE. 2010; 98:666–687.

Kerr YH, Waldteufel P, Richaume P, Wigneron JP, Ferrazzoli P, Mahmoodi A, Al Bitar A, Cabot F, Gruhier C, Juglea SE, Leroux D, Mialon A, Delwart S. The SMOS Soil Moisture Retrieval Algorithm. IEEE Transactions on Geoscience and Remote Sensing. 2012; 50:1384–1403.

Kerr YH, Al-Yaari A, Rodriguez-Fernandez N, Parrens M, Molero B, Leroux D, Bircher S, Mahmoodi A, Mialon A, Richaume P, Delwart S, Al Bitar A, Pellarin T, Bindlish R, Jackson TJ, Rüdiger C, Waldteufel P, Mecklenburg S, Wigneron JP. Overview of SMOS performance in terms of global soil moisture monitoring after six years in operation. Remote Sensing of Environment. 2016; 180:40–63.

Kolassa J, Aires F, Polcher J, Prigent C, Jimenez C, Pereira JM. Soil moisture retrieval from multi-instrument observations: Information content analysis and retrieval methodology. Journal of Geophysical Research: Atmospheres. 2013; 118:4847–4859.

Larson KM, Small EE, Gutmann ED, Bilich AL, Braun JJ, Zavorotny VU. Use of GPS receivers as a soil moisture network for water cycle studies. Geophysical Research Letters. 2008; 35 n/a-n/a.

Liu YY, Dorigo WA, Parinussa RM, de Jeu RAM, Wagner W, McCabe MF, Evans JP, van Dijk AIJM. Trend-preserving blending of passive and active microwave soil moisture retrievals. Remote Sensing of Environment. 2012; 123:280–297.

Lv S, Zeng Y, Wen J, Su Z. A reappraisal of global soil effective temperature schemes. Remote Sensing of Environment. 2016; 183:144–153.

Mo T, Choudhury BJ, Schmugge TJ, Wang JR, Jackson TJ. A model for microwave emission from vegetation-covered fields. Journal of Geophysical Research: Oceans. 1982; 87:11229–11237.

Njoku EG, Li L. Retrieval of land surface parameters using passive microwave measurements at 6–18 GHz. IEEE Transactions on Geoscience and Remote Sensing. 1999; 37:79–93.

Njoku EG, Wilson WJ, Yueh SH, Dinardo SJ, Fuk KL, Jackson TJ, Lakshmi V, Bolten J. Observations of soil moisture using a passive and active low-frequency microwave airborne sensor during SGP99. IEEE Transactions on Geoscience and Remote Sensing. 2002; 40:2659–2673.

Njoku EG, Jackson TJ, Lakshmi V, Chan TK, Nghiem SV. Soil moisture retrieval from AMSR-E. IEEE Transactions on Geoscience and Remote Sensing. 2003; 41:215–229.

Oliva R, Daganzo E, Kerr YH, Mecklenburg S, Nieto S, Richaume P, Gruhier C. SMOS Radio Frequency Interference Scenario: Status and Actions Taken to Improve the RFI Environment in the

1400–1427-MHz Passive Band. IEEE Transactions on Geoscience and Remote Sensing. 2012; 50:1427–1439.

Oliva R, Daganzo E, Richaume P, Kerr Y, Cabot F, Soldo Y, Anterrieu E, Reul N, Gutierrez A, Barbosa J, Lopes G. Status of Radio Frequency Interference (RFI) in the 1400–1427 MHz passive band based on six years of SMOS mission. Remote Sensing of Environment. 2016; 180:64–75.

Owe M, Van de Griend AA. Comparison of soil moisture penetration depths for several bare soils at two microwave frequencies and implications for remote sensing. Water Resources Research. 1998; 34:2319–2327.

Owe M, de Jeu R, Walker J. A methodology for surface soil moisture and vegetation optical depth retrieval using the microwave polarization difference index. IEEE Transactions on Geoscience and Remote Sensing. 2001; 39:1643–1654.

Parinussa RM, Holmes TRH, Yilmaz MT, Crow WT. The impact of land surface temperature on soil moisture anomaly detection from passive microwave observations. Hydrology and Earth System Sciences. 2011; 15:3135–3151.

Parrens M, Zakharova E, Lafont S, Calvet JC, Kerr Y, Wagner W, Wigneron JP. Comparing soil moisture retrievals from SMOS and ASCAT over France. Hydrology and Earth System Sciences. 2012; 16:423–440.

Parrens M, Wigneron JP, Richaume P, Mialon A, Al Bitar A, Fernandez-Moran R, Al-Yaari A, Kerr YH. Global-scale surface roughness effects at L-band as estimated from SMOS observations. Remote Sensing of Environment. 2016; 181:122–136.

Piepmeier J, Mohammed P, De Amici G, Kim E, Peng J, Ruf C, Hanna M, Yueh S, Entekhabi D. Soil Moisture Active Passive (SMAP) Project Algorithm Theoretical Basis Document SMAP L1B Radiometer Data Product: L1B_TB. 2016

Rautiainen K, Lemmetyinen J, Pulliainen J, Vehvilainen J, Drusch M, Kontu A, Kainulainen J, Seppanen J. L-Band Radiometer Observations of Soil Processes in Boreal and Subarctic Environments. IEEE Transactions on Geoscience and Remote Sensing. 2012; 50:1483–1497.

Reichle R, Draper C, Koster R, Liu A, Girotto M, Mahanama S, De Lannoy G. Assessment of MERRA-2 land surface hydrology estimates. Journal of Climatology. 2016 submitted.

Reichle RH, Koster RD, De Lannoy GJM, Forman BA, Liu Q, Mahanama SPP, Touré A. Assessment and Enhancement of MERRA Land Surface Hydrology Estimates. Journal of Climate. 2011; 24:6322–6338.

Rondinelli WJ, Hornbuckle BK, Patton JC, Cosh MH, Walker VA, Carr BD, Logsdon SD. Different Rates of Soil Drying after Rainfall Are Observed by the SMOS Satellite and the South Fork in situ Soil Moisture Network. Journal of Hydrometeorology. 2015; 16:889–903.

Saleh K, Wigneron JP, de Rosnay P, Calvet JC, Kerr Y. Semi-empirical regressions at L-band applied to surface soil moisture retrievals over grass. Remote Sensing of Environment. 2006; 101:415–426.

Sanchez N, Martinez-Fernandez J, Scaini A, Perez-Gutierrez C. Validation of the SMOS L2 Soil Moisture Data in the REMEDHUS Network (Spain). Geoscience and Remote Sensing, IEEE Transactions on. 2012; 50:1602–1611.

Schaefer GL, Cosh MH, Jackson TJ. The USDA Natural Resources Conservation Service Soil Climate Analysis Network (SCAN). Journal of Atmospheric and Oceanic Technology. 2007; 24:2073–2077.

Schmugge T, Wilheit T, Webster W Jr, Gloersen P. Remote sensing of soil moisture with microwave radiometers-II. Nat Aeronautics and Space Admin, NASA Tech Note D-8321. 1976

Seneviratne SI, Corti T, Davin EL, Hirschi M, Jaeger EB, Lehner I, Orlowsky B, Teuling AJ. Investigating soil moisture–climate interactions in a changing climate: A review. Earth-Science Reviews. 2010; 99:125–161.

Smith AB, Walker JP, Western AW, Young RI, Ellett KM, Pipunic RC, Grayson RB, Siriwardena L, Chiew FHS, Richter H. The Murrumbidgee soil moisture monitoring network data set. Water Resources Research. 2012; 48:W07701.

Tagesson T, Fensholt R, Guiro I, Rasmussen MO, Huber S, Mbow C, Garcia M, Horion S, Sandholt I, Holm-Rasmussen B, Göttsche FM, Ridler ME, Olén N, Lundegard Olsen J, Ehammer A, Madsen M, Olesen FS, Ardö J. Ecosystem properties of semiarid savanna grassland in West Africa and its

NASA Author Manuscript

NASA Author Manuscript

NASA Author Manuscript

relationship with environmental variability. Global Change Biology. 2015; 21:250–264. [PubMed: 25204271]

Taylor KE. Summarizing multiple aspects of model performance in a single diagram. Journal of Geophysical Research: Atmospheres. 2001; 106:7183–7192.

Ulaby FT, Dubois PC, van Zyl J. Radar mapping of surface soil moisture. Journal of Hydrology. 1996; 184:57–84.

Van der Schalie R, Kerr YH, Wigneron JP, Rodríguez-Fernández NJ, Al-Yaari A, Jeu RAMd. Global SMOS Soil Moisture Retrievals from The Land Parameter Retrieval Model. International Journal of Applied Earth Observation and Geoinformation, 45, Part B. 2016:125–134.

Vittucci C, Ferrazzoli P, Kerr Y, Richaume P, Guerriero L, Rahmoune R, Laurin GV. Smos retrieval over forests: Exploitation of optical depth and tests of soil moisture estimates. Remote Sensing of Environment. 2016; 180:115–127.

Wagner, W., Dorigo, W., de Jeu, Richard, Fernandez, Diego, Benveniste, Jerome, Haas, Eva, Ertl, M. Fusion of Active and Passive Microwave Observations to Create an Essential Climate Variable Data Record on Soil Moisture. XII Congress of the International Society for Photogrammetry and Remote Sensing-Melbourne; Australia. 2012.

Wang JR, Choudhury BJ. Remote sensing of soil moisture content, over bare field at 1.4 GHz frequency. Journal of Geophysical Research: Oceans. 1981; 86:5277–5282.

Wang JR, O'Neill PE, Jackson TJ, Engman ET. Multifrequency Measurements of the Effects of Soil Moisture, Soil Texture, And Surface Roughness. IEEE Transactions on Geoscience and Remote Sensing, GE-21. 1983:44–51.

Western AW, Zhou SL, Grayson RB, McMahon TA, Blöschl G, Wilson DJ. Spatial correlation of soil moisture in small catchments and its relationship to dominant spatial hydrological processes. Journal of Hydrology. 2004; 286:113–134.

Wigneron JP, Chanzy A, Calvet JC, Bruguier N. A simple algorithm to retrieve soil moisture and vegetation biomass using passive microwave measurements over crop fields. Remote Sensing of Environment. 1995; 51:331–341.

Wigneron JP, Calvet JC, Pellarin T, Van de Griend AA, Berger M, Ferrazzoli P. Retrieving near-surface soil moisture from microwave radiometric observations: current status and future plans. Remote Sensing of Environment. 2003; 85:489–506.

Wigneron JP, Calvet JC, De Rosnay P, Kerr Y, Waldteufel P, Saleh K, Escorihuela MJ, Kruszewski A. Soil moisture retrievals from biangular L-band passive microwave observations. Geoscience and Remote Sensing Letters, IEEE. 2004; 1:277–281.

Wigneron JP, Kerr Y, Waldteufel P, Saleh K, Escorihuela MJ, Richaume P, Ferrazzoli P, de Rosnay P, Gurney R, Calvet JC, Grant JP, Guglielmetti M, Hornbuckle B, Mätzler C, Pellarin T, Schwank M. L-band Microwave Emission of the Biosphere (L-MEB) Model: Description and calibration against experimental data sets over crop fields. Remote Sensing of Environment. 2007; 107:639–655.

Wigneron JP, Chanzy A, Kerr YH, Lawrence H, Shi J, Escorihuela MJ, Mironov V, Mialon A, Demontoux F, Rosnay Pd, Saleh-Contell K. Evaluating an Improved Parameterization of the Soil Emission in L-MEB. IEEE Transactions on Geoscience and Remote Sensing. 2011; 49:1177–1189.

Zeng J, Chen KS, Bi H, Chen Q. A Preliminary Evaluation of the SMAP Radiometer Soil Moisture Product Over United States and Europe Using GroundBased Measurements. IEEE Transactions on Geoscience and Remote Sensing. 2016:1.
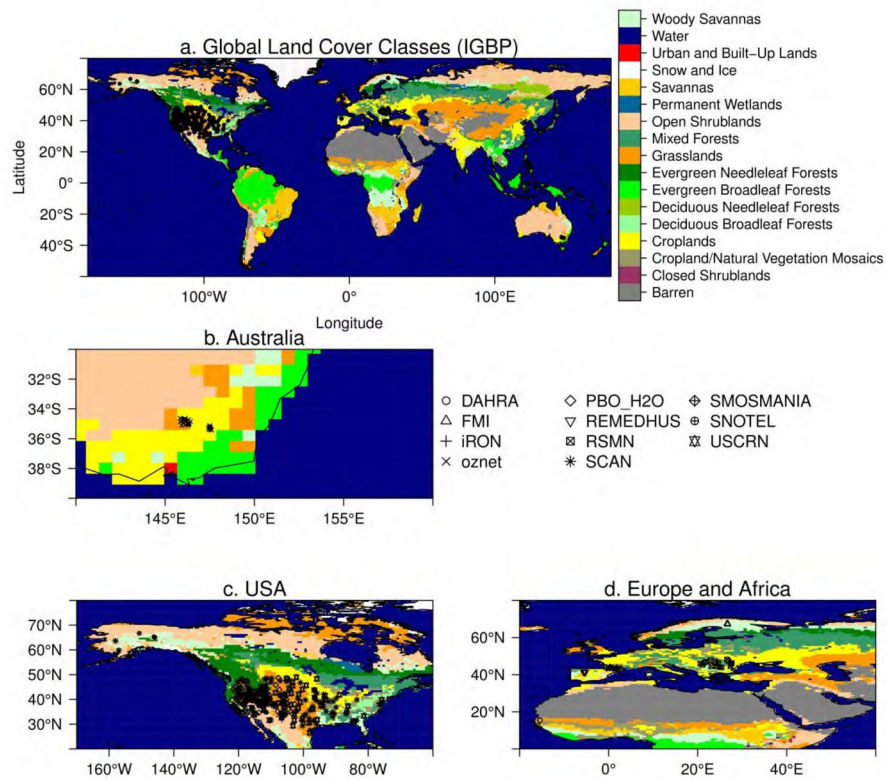
Fig. 1.

IGBP (International Geosphere Biosphere Programme) land cover classification (Friedl et al., 2010) with the locations of the different *in situ* soil moisture sites (a) over Australia (b), the USA (c), and Africa and Europe (d).
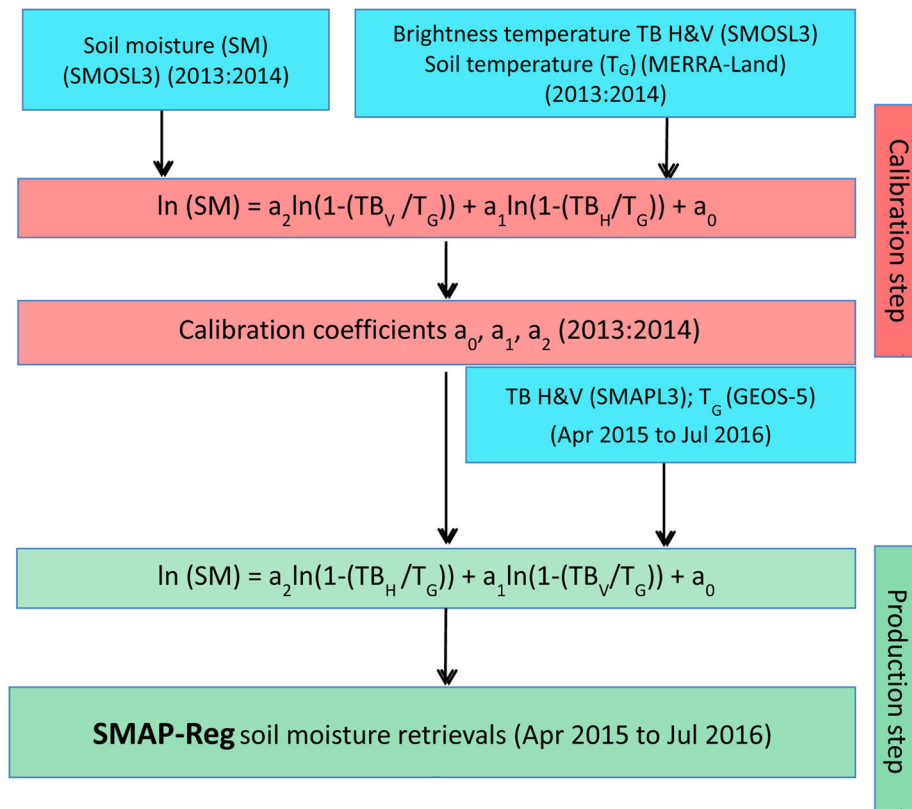
Fig. 2.
The LRM (local regression method) algorithm: inputs (in blue), calibration step (in red), and soil moisture production step (in green).
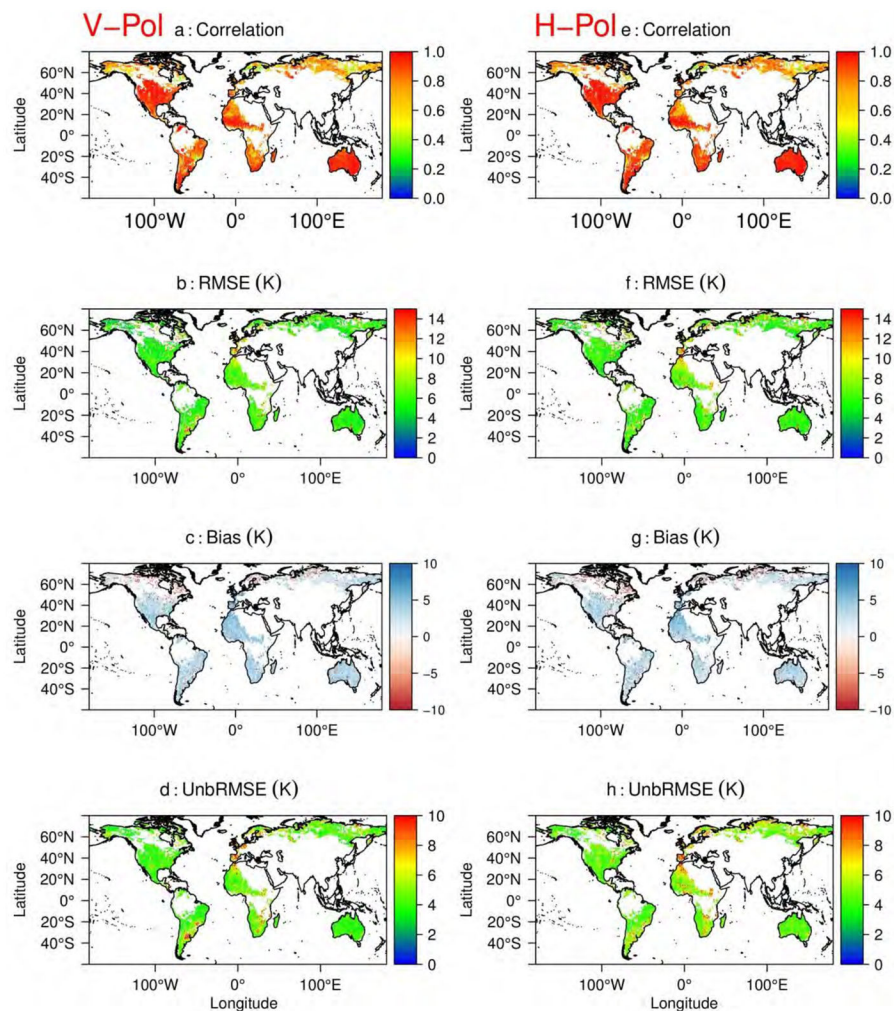
Fig. 3.
Global inter-comparison between SMOS and SMAP TBs during the Apr 2015–Jul 2016 at both polarizations vertical (V-pol; left) and horizontal (H-pol; right): (a & e) correlation, (b & f) RMSE, (c & g) Bias, and (d &h) UnbRMSE. Pixels with a number of observations lower than 15 are indicated as blank areas.
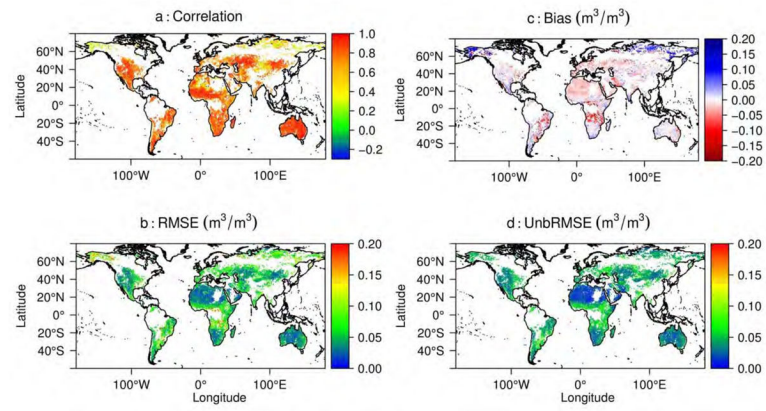
Fig. 4.
Global inter-comparison between SMOS and SMAP soil moisture retrievals during the Apr 2015–Jul 2016: (a) correlation, (b) RMSE, (c) Bias, and (d) UnbRMSE. Pixels with a number of observations lower than 15 are indicated as blank areas.
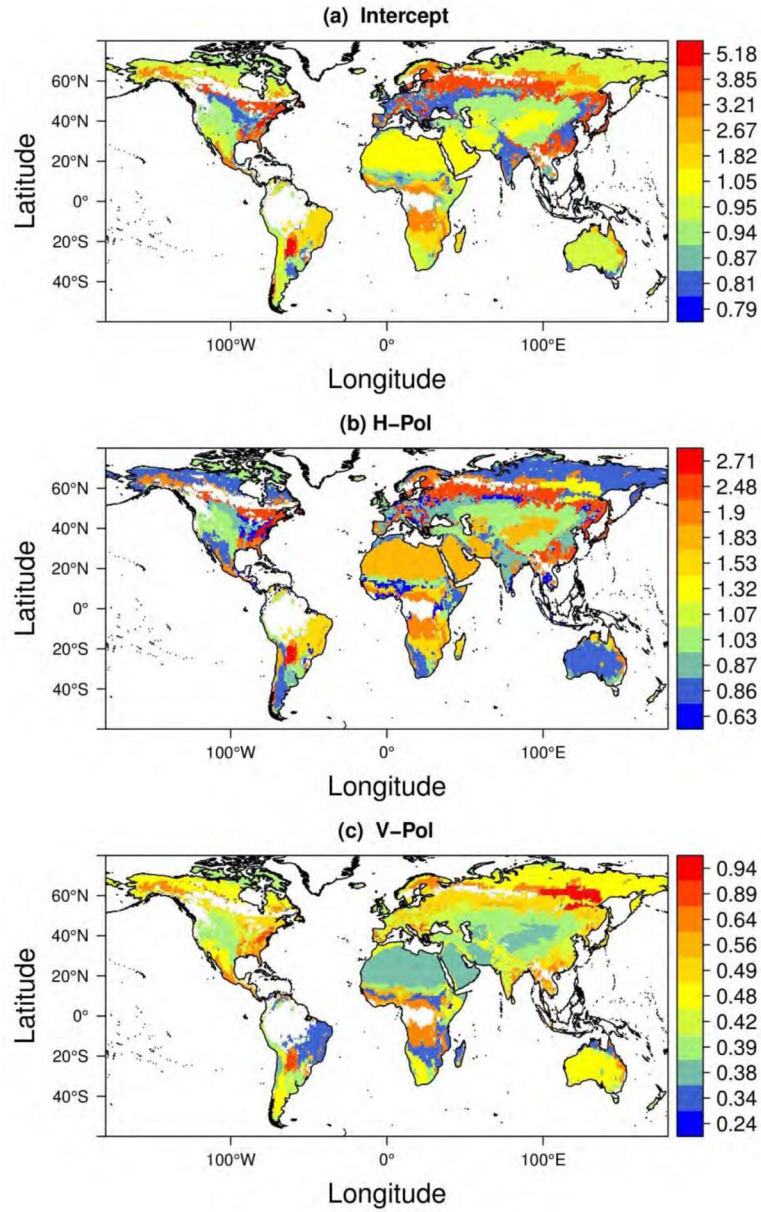
Fig. 5.
Regression coefficients of Eq. 1 calibrated using SMOS Level 3 TB and soil moisture in 2013–2014 (a): intercept (a_0), (b) slope of regression line corresponding to the horizontal polarization (a_1), and (c) slope of regression line corresponding to the vertical polarization (a_2).
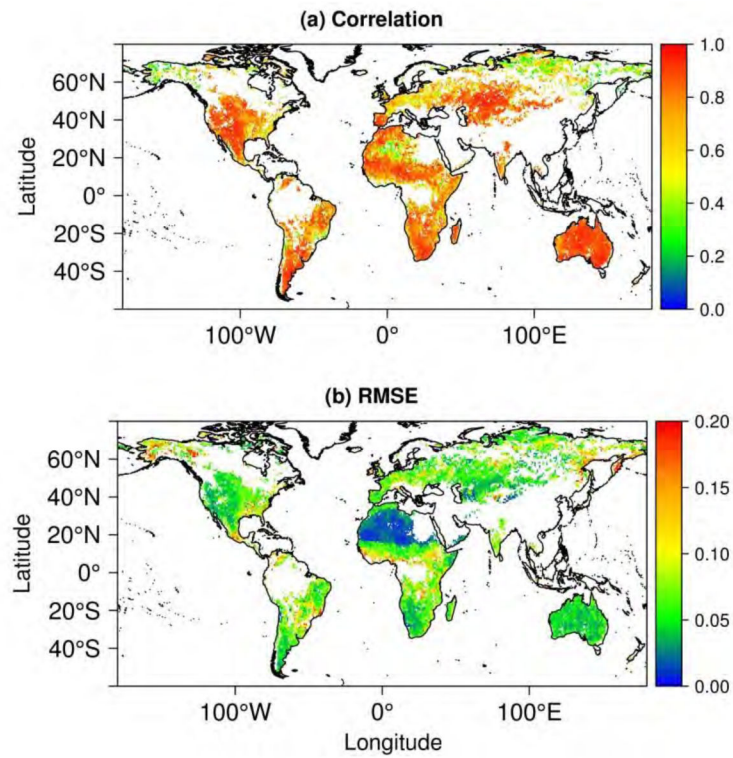
Fig. 6.
Comparison between the soil moisture values computed from the SMOS TB data using LRM (SMOS_Reg) and the SMOS official level 3 soil moisture product in 2013–2014: (a) correlation, R and (b) RMSE (m^3/m^3). Pixels with a number of observations lower than 15 are indicated as blank areas.
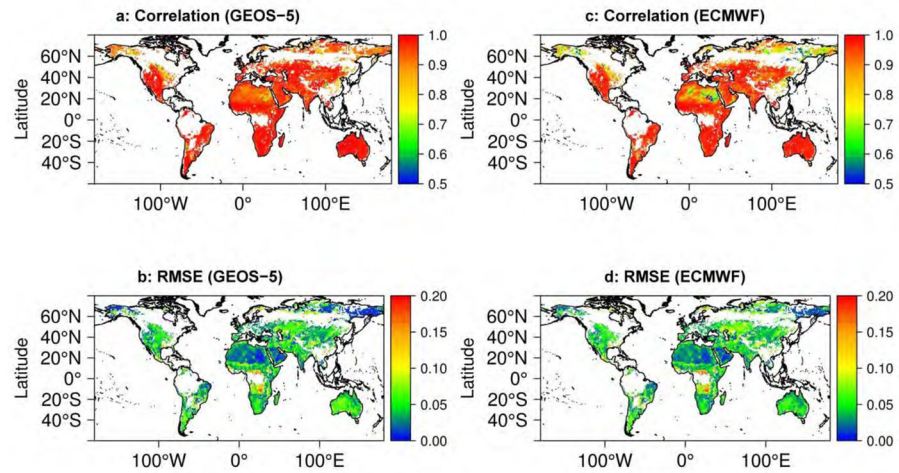
Fig. 7.

Comparison between the SMAP-derived soil moisture applying LRM (SMAP_Reg) using two different soil temperature products: GEOS-5 (left) and ECMWF (right) and the SMAP level 3 soil moisture product (SMAP_SCA) from Apr 2015 to Jul 2016: (top) correlation, R (−) and (bottom) RMSE (m^3/m^3).
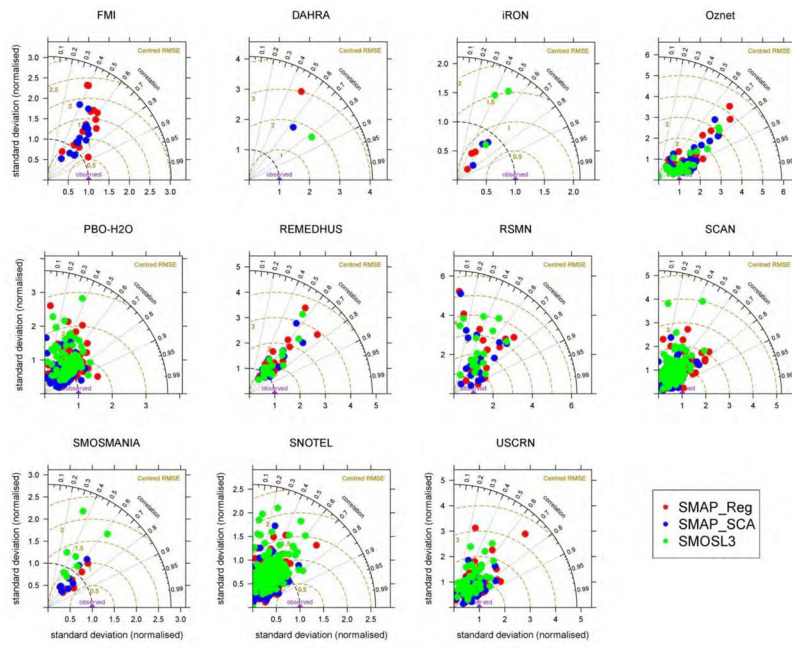
Fig. 8.
Taylor's diagrams for SMAP_Reg (in red), SMAP_SCA (in blue), and SMOSL3 (in green) over the FMI, DAHRA, iRON, and Oznet (upper panel), over SCAN, PBO-H2O, REMEDHUS, and RSMN sites (middle panel), and over SNOTEL, USCRN, and SMOSMANIA sites (lower panel).

Fig. 9.
Bar charts showing Bias (m³/m³), R, RMSE (m³/m³), and UnbRMSE (m³/m³) between
SMAP_SCA (in blue), SMAP_Reg (in red), and SMOSL3 (in green) and the observed soil
moisture over the 11 networks used in this study.

Table 1

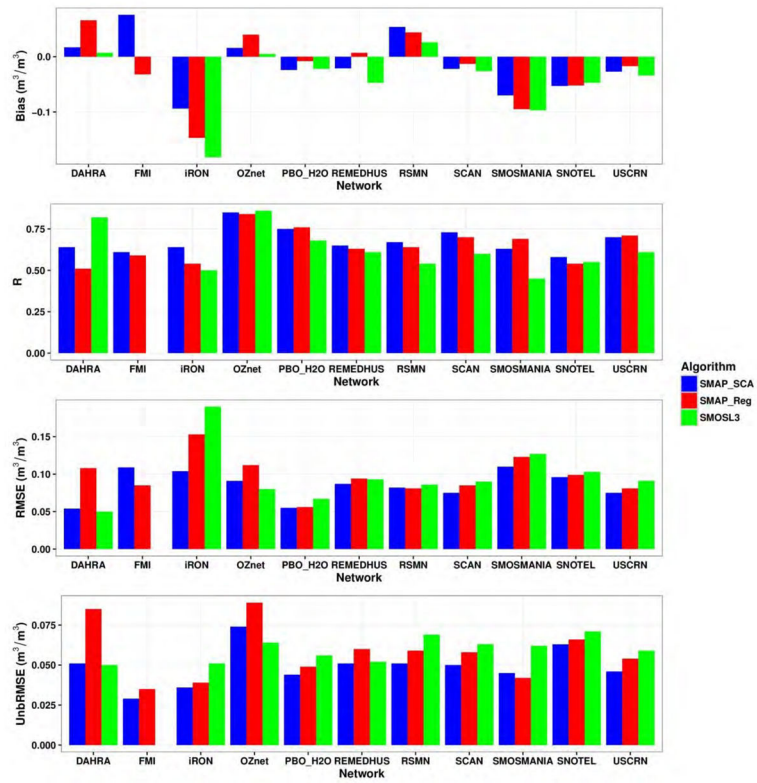Regression coefficients of Eq. 1 calibrated using SMOS Level 3 TB and soil moisture in 2013–2014: a_0 represents the intercept, a_1 and a_2 represent the slope of regression line corresponding to H-pol and V- pol, respectively.

Land cover class	a_0	a_1	a_2
Deciduous Needleleaf forest	2.671	1.322	0.937
Deciduous Broadleaf forest	5.184	2.713	0.889
Mixed forest	3.848	2.485	0.492
Closed shrublands	0.789	1.068	0.242
Open shrublands	0.952	0.864	0.478
Woody savannas	3.212	1.903	0.643
Savannas	1.821	1.534	0.336
Grasslands	0.937	1.032	0.391
Croplands	0.815	0.867	0.421
Cropland/Natural vegetation mosaic	0.874	0.626	0.558
Barren or sparsely vegetated	1.049	1.830	0.384

Table 2

Statistics of the evaluation of the SMAP_Reg, SMAP_SCA, and SMOSL3 against ground based measurements. The average (median for R instead of "average" as correlation is not additive) values were only computed for sites that have p_value < 0.05 and number of observations was higher than 15.

Matric	Bias (m³/m³) (mean)			RMSE (m³/m³) (mean)			R (median)			UnbRMSE (m³/m³) (mean)		
Algorithm / Network (No of sites)	SMAP_SCA	SMAP_Reg	SMOS L3	SMAP_SCA	SMAP_Reg	SMOS L3	SMAP_SCA	SMAP_Reg	SMOS L3	SMAP_SCA	SMAP_Reg	SMOS L3
REMEDHUS (19)	−0.021	**0.007**	−0.047	**0.087**	0.094	0.093	**0.65**	0.63	0.61	**0.051**	0.060	0.052
PBO_H2O (76)	−0.024	**−0.008**	−0.022	**0.055**	0.056	0.067	0.75	**0.76**	0.68	**0.044**	0.049	0.056
RSMN (16)	0.054	0.044	**0.026**	0.082	**0.081**	0.086	**0.67**	0.64	0.54	**0.051**	0.059	0.069
SCAN (104)	−0.022	**−0.013**	−0.026	**0.075**	0.085	0.090	**0.73**	0.70	0.60	**0.050**	0.058	0.063
SNOTEL (125)	−0.053	−0.052	**−0.047**	**0.096**	0.099	0.103	**0.58**	0.54	0.55	**0.063**	0.066	0.071
USCRN (51)	−0.027	**−0.017**	−0.034	**0.075**	0.081	0.091	0.70	**0.71**	0.61	**0.046**	0.054	0.059
FMI (14)	0.076	**−0.032**	-	0.109	**0.085**	-	**0.61**	0.59	-	**0.029**	0.035	-
iRON (3)	**−0.094**	−0.147	−0.182	**0.104**	0.153	0.190	**0.64**	0.54	0.50	**0.036**	0.039	0.051
DAHRA (1)	0.017	0.066	**0.007**	0.054	0.108	**0.050**	0.64	0.51	**0.82**	0.051	0.085	**0.050**
SMOSMANIA (7)	**−0.070**	−0.095	−0.097	**0.110**	0.123	0.127	0.63	**0.69**	0.45	0.045	**0.042**	0.062
Oznet (34)	0.016	0.040	**0.005**	0.091	0.112	**0.080**	0.85	0.84	**0.86**	0.074	0.089	**0.064**